Spin-spin interaction in ε-$VOPO_4$ through doping light elements

Byungkyun Kang and Qiang Zhu*

Department of Physics and Astronomy, University of Nevada, Las Vegas, NV 89154, USA

E-mail: qiang.zhu@unlv.edu

Abstract

Non-magnetic transition metal oxides are usually magnetized by doping magnetic metallic elements. Here, we propose an alternative route to achieve magnetization by doping non-magnetic H and Li atoms. Using vanadium oxides ($VOPO_4$) as an example, we find that the doping of H and Li can effectively localize the excess electrons on V-d orbitals. As such, non-magnetic ε-$VOPO_4$ is predicted to posses short-range spin-spin interaction. When the doped H_2 molecules are bonded with the axial oxygen, we observe a notable charge transfer from oxygen to vanadium. The transferred electrons are localized on two adjacent VO_6 octahedrons and induce the spin-spin interaction. We further show that H_2 dopants in ε-$VOPO_4$ tends to be dispersed with a homogeneous magnetization. Our results suggest that H_2-doped ε-$VOPO_4$ can be utilized in the field of spintronics.

Keywords

spin-spin interaction, defect, spintronics

INTRODUCTION

Vanadium phosphorus oxide (VPO) is an attractive material as catalyst for selective oxidation of alkanes[1–3] or cathode materials in the Li-ion batteries.[4–8] However, there is little study on its application in optoelectric or spintronic devices. Recently, several transition metal oxides, such as ZnO and TiO_2 have received considerable interests for applications as the diluted magnetic semiconductors.[9,10] An experiment demonstrates that a slight doping of transition metal ions in non-magnetic ZnO induces ferromagnetic ordering at room temperature.[11] In TiO_2, the Co and Ni dopants, associated with oxygen vacancies, also give rise to room temperature ferromagnetism.[10,12] From the theoretical perspective, a density functional theory (DFT) study by Wang et al. shows that substitutional dopants of Cr, Fe, Co, and Ni in ZnO can couple antiferromagnetically.[13] Another recent DFT work suggests that spins in Cr-doped Li_xVOPO_4 can couple ferromagnetically.[14]

However, the strong *d*-*d* interactions between metal dopants often results in the formation of metal clusters, thus leading to an inhomogenous magnetization.[15,16] For operational applications, it often requires a magnetic orientation without aggregation of dopants, which has led to non-magnetic elements doping or vacancy induced magnetism in non-magnetic oxides.[9,17] Sometimes, hydrogen was introduced into transition metal oxides to control the magnetism. It has been found that hydrogen doping can stabilize Zn vacancies and give rise to the vacancy-induced magnetism in ZnO.[9] Nevertheless, it was found that further substitution of H at the Zn site leads to a reduced net magnetic moment.[18]

In comparison to TiO_2, ε-$VOPO_4$ has a similar electronic structure with empty states of transition metal-*d*. The calculated band gap values of ε-$VOPO_4$ range from 1.94 to 2.99 eV.[5,19] In addition, the recent experiment confirmed that there is no magnetism induced by transition metal in ε-$VOPO_4$.[20] Hence, the bulk ε-$VOPO_4$ is electronically analogical to TiO_2. It is reasonable to speculate that the magnetism can also be induced by chemical doping. Furthermore, the ε-$VOPO_4$ has a flexible and open one dimensional (1D) structure framework that is featured by the corner sharing VO_6 octahedrons. This structure framework is expected to allow easy lattice distortion coupling with excess electrons, as suggested by the recent observation of small electron polaron in ε-$VOPO_4$.[5] When the dopants are introduced, the excess electrons can be held by the octahedron via lattice distortion and thus may give rise to the magnetism.

Following the aforementioned reasoning, we performed a systematic first-principles investigation on the doping effect of ε-$VOPO_4$. We found that doping non-magnetic H, H_2 and Li on ε-$VOPO_4$ can effectively localize the excess electrons on V-d orbitals and induce the magnetization. Remarkably, doping the interstitial H_2 is found to induce the shot-range spin-spin interaction. Unlike that doping of magnetic elements often introduce the aggregation of dopants, we found that the H_2 dopants in ε-$VOPO_4$ result in a homogeneous magnetization. Our simulation suggests that the doped ε-$VOPO_4$ is feasible for spintronic applications.

Computational Methods

All calculations were carried out using the projector augmented wave method as implemented within the plane-wave code VASP.[21–23] We used the Generalized Gradient Approximation (GGA) with Perdew, Burke and Ernzerhof (PBE) functional,[24] with a Hubbard U correction to treat strong correlation of V-d electrons. All calculations have a uniform energy cutoff of 520 eV, and forces are converged within 0.03 eV/Å. We have used a 4×4×4 Γ-centered k-point grid for geometry relaxation. Using U = 3.25 eV, the fully relaxed cell parameters are a = 7.345, b = 7.066 and c = 7.388 Å, α = 90.0, β = 115.3, and γ = 90.0°. We also checked the results with U = 2.0 and 4.0 eV and did not observe any notable change. Our optimized cell parameters agree with the recent works based on the DFT+U approach,[14,25] but slightly differ from the experimental values of a = 7.265, b = 6.893, c = 7.265 Å, (α = 90.0, β = 115.3, γ = 90.0°).[26] Using the optimized structure, we constructed a 3×3×3 supercell (378 atoms) for the subsequent defect calculations, in which a single k-point at the fractional coordinate (0.25, 0.25, 0.25) in reciprocal space was used for sampling the

Brillouin zone. To test the effect of van der Waals dispersion, we conducted dispersion corrected calculations with DFT-D3 method. The fully relaxed lattice parameters are a = 7.321 Å, b = 7.018 Å and c = 7.334 Å, $\alpha = 90.0°$, $\beta = 115.9°$, and $\gamma = 90.0°$. They are very close to the relaxed lattice parameters without DFT-D3. We repeated the calculations to find short-range exchange interaction using the lattice constants calculated within the DFT-D3 method. The calculated exchange energy of 27 meV is exactly same as the one without DFT-D3. This indicates that the inclusion of dispersion correction does not affect the main results.

In case of single H or Li doped ε-$VOPO_4$, we set initial local magnetic moment of 1.5 μ_B for all V without modifying the atomic configuration. For two H atoms doped ε-$VOPO_4$, we set initial local magnetic moment of ±1.5 μ_B for V near the H without modifying the atomic configuration as well. For H_2 molecules doped ε-$VOPO_4$, we set initial ±1.5 μ_B for V near the H_2 and modified the atomic configuration at the same time, which resulted in three local minima (see Doping of two H atoms section). The purpose of modification is to change the axial V-O bond lengths by moving the V atoms along the long axis in VO_6 octahedron.

RESULTS AND DISCUSSIONS

Electronic and structural properties of ε-$VOPO_4$

ε-$VOPO_4$ crystallizes in monoclinic symmetry (space group Cc) with a unit cell consisting of 28 atoms.[26] Figure 1 (a) shows the optimized structure with the highlighted VO_6 octahedrons and PO_4 tetrahedrons. Since this structure does not have the centrosymmetry, the octahedrons deviate from the ideal O_h point group symmetry with an elongated polar axis (while the other four V-O bonds form an equator). In each VO_6 octahedron, one axial V-O bond (2.57 Å) is longer than the other (1.61 Å), whereas four equatorial V-O bonds have roughly the same lengths ($\sim$1.90 Å). In ε-$VOPO_4$, the VO_6 octahedrons share oxygen atoms at axial corners and form the 1D chains. Additionally, the VO_6 octahedrons are connected to

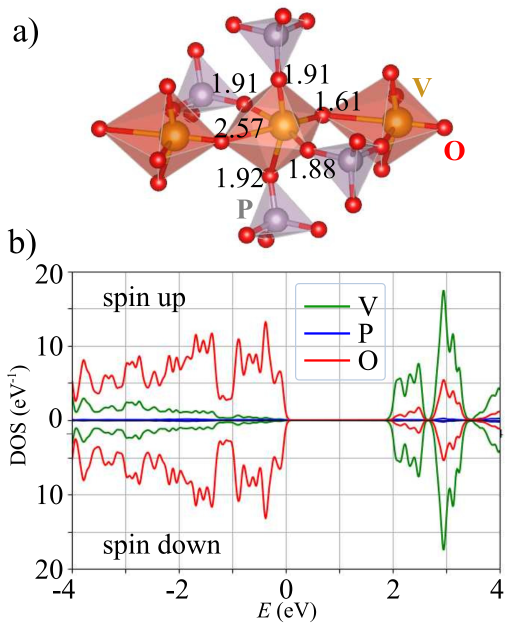

Figure 1: a) Optimized structure of VO_6 octahedron in ε-$VOPO_4$. The bond lengths of V-O are presented in units of Å. b) Spin-polarized atom-projected density of states. The valance band maximum is set to zero.

the neighboring PO_4 tetrahedrons by sharing equatorial oxygen atoms. Figure 1 (b) displays the spin-polarized atom-resolved density of states (DOS), which are identical for both spin up and down states. Hence, there is no net magnetic moment in crystalline ε-$VOPO_4$. The valance (conduction) band is mainly comprised of O-p (V-d) orbital characters. Both bands exhibit small but notable hybridization between O-p and V-d orbitals. The calculated band structures (data not shown) exhibit the indirect band gaps of 1.56, 1.76, 1.93 and 2.01 eV for $U=$ 0.0, 2.0, 3.25 and 4.0 eV, respectively. According to the calculated DOS, there is small portion of V-d character in the valance band, and the calculated local magnetic moment on V is zero. These results suggest an approximate V^{5+} ionic state in perfect ε-$VOPO_4$, agreeing with the recent magnetic susceptibility measurement data .[20]

Doping of single H atom

For H doped ε-$VOPO_4$, we tested two configurations of distinct choices of interstitial sites, (i) one near the equatorial oxygen (O_{equ}) and (ii) near the corner oxygen (O_{cor}). Figure 2

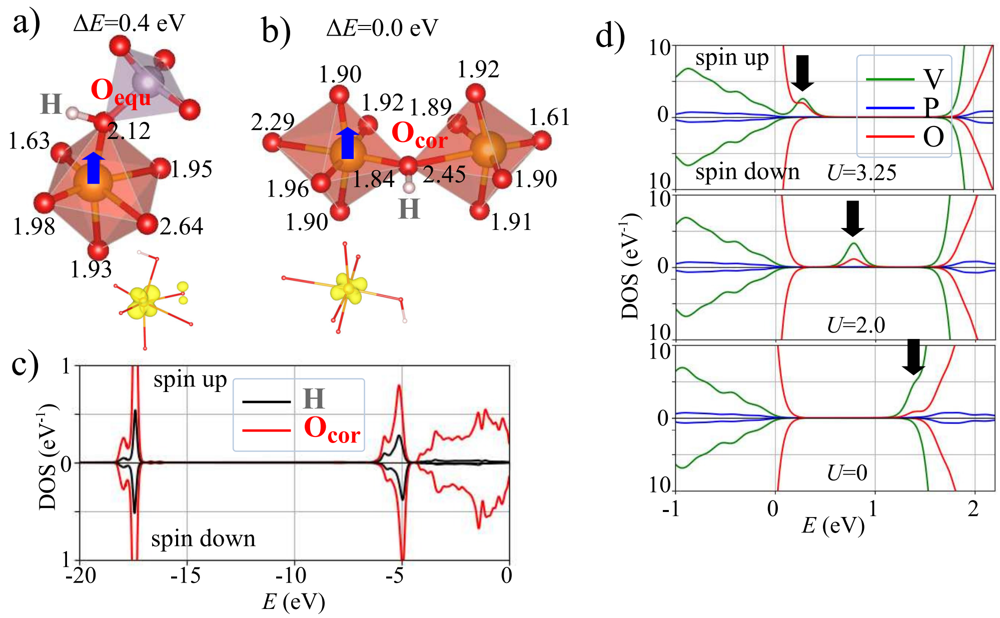

Figure 2: (a) and (b) show the optimized VO_6 octahedrons in ε-$VOPO_4$ with two choices of hydrogen dopants near the corner and equtorial oxygens. Blue arrows denote localized excess electrons upon H doping. The bond lengths of V-O are presented in units of Å. ΔE is the total energy difference between configurations. Spin density associated with the V-d state is presented. c) Spin-polarized H and corner oxygen-projected density of states of configuration (b). d) Spin-polarized atom-projected density of states as a function of U (eV). Defect states are marked in black arrows. The valance band maximum is set to zero. Hydrogen projected density of states are not shown here due to their absent in the selected energy range.

(a) shows the first configuration. After optimization, it is clear that electrons are localized into the octahedron. The local magnetic moment on V-d (marked by blue arrow) in the octahedron is 1.045 μ_B. The H doping also increased equatorial V-O_{equ} bond length from 1.91 to 2.21 Å to due to the excess electrons. Figure 2 (b) shows the second configuration where the interstitial H is near the corner oxygen. Compared to the first configuration, its energy is 0.4 eV lower. Thus, we focused on the latter configuration. The major lattice distortion is found at the left VO_6 octahedron (marked by blue arrow) where V moves $\sim$0.25 Å away from O_{cor}. This configuration also has localized electrons on V-d in the left VO_6 octahedron, with a local magnetic moment of 1.028 μ_B. Formation of strong O_{cor}-H bond is manifested by peaks at $\sim$-17 and $\sim$-5 eV in the DOS (see Fig. 2 (c)), that correspond to the bonding states of the O_{cor}-H. This leads to a charge transfer from O_{cor} to V. In consequence, the transferred charges are localized on V-d and form the defect state in the band gap as shown in Fig. 2 (d). This defect state is reminiscent of electron polarons in Cs_2HfCl_6[27] and Cs_4PbBr_6.[28] However, the electron carriers are trapped in an octahedron in the presence of short-range electron-phonon coupling in those materials. For H doped ε-$VOPO_4$, the transferred charges by H doping is localized in an octahedron with significant local lattice distortion.

Figure 2 (d) shows the defect states induced by the interstitial H dopant near O_{cor}, as a function of effective on-site Coulomb interactions U. When $U = 0$, the energy level of the defect state is near the conduction band minimum. The defect state is found to continuously shift towards the valance band maximum with the increment of U values. The local magnetic moment on V-d in the distorted octahedron is $\sim$1.0 μ_B when $U \geq 2.0$ eV, whereas it is 0.7 μ_B in the same octahedron and small moments (~ 0.1 μ_B) appear on the neighbor octahedron when $U = 0$ eV. Therefore, a sufficient U value is necessary to localize electron on V-d. And the energy level of defect state in the gap strongly depends the U. In two relevant studies, it was found that doping H to $BaTiO_3$[29] and TiO_2[30] also led to the formation of defect states contributed from Ti-d and O-p at the conduction band minimum. However, those calculations did not include U. It is expected that the defect states in those materials will shift towards the valance band maximum as well.

Doping of two H atoms

To investigate the interaction between localized electrons, we considered doping two H atoms on the same interstitial site. The spin-spin interaction between the localized electrons is estimated by calculating the exchange energy from the total energy difference between antiferromagnetic (AFM) and ferromagnetic (FM) states. Figure 3 shows four possible atomic and spin configurations of two H doping in a VO_6 octahedron chain, as well as their energy differences. The most stable ($\Delta E = 0$ eV) configuration and spin orientation is shown in the top panel of Fig. 3, where two interstitial H near the corner oxygens localize two electrons on

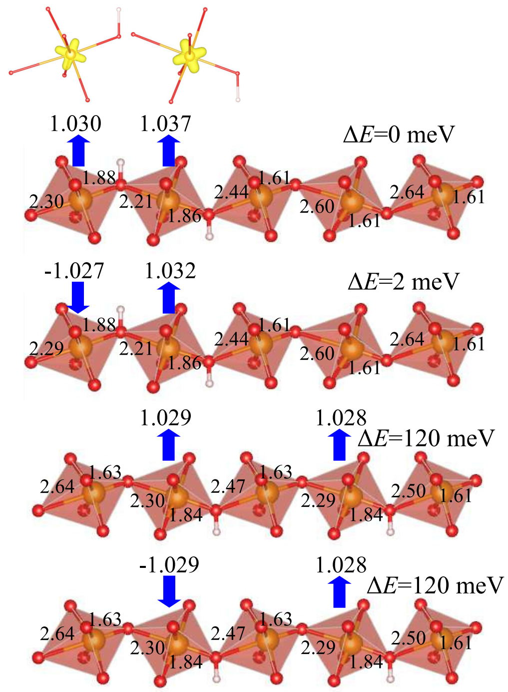

Figure 3: Optimized structure of VO_6 octahedrons in ε-$VOPO_4$ with two hydrogens dopants. Blue arrows denote localized excess electrons. Local magnetic moments on V-d are presented in units of μ_B on top of the arrows. The bond lengths of V-O are presented in units of Å. ΔE is the total energy difference between configurations. For top model, spin density associated with the V-d state is presented.

V-d in adjacent two octahedrons. Both local spin moments align ferromagnetically with local magnetic moments of $\sim$1.0 μ_B. The same configuration with AFM ordering is 2 meV higher than the FM ordering in energy, indicating a negligible spin-spin interaction on this atomic configuration. The other atomic configuration (see the two lower panels of Fig. 3), with two H atoms at two separated octahedrons, also show negligible energy difference between the FM and AFM orderings. However, its total energy is 120 meV higher than that of the first configuration. It suggests that the lattice distortion in the first configuration localize two electron more efficiently, and hydrogen atoms in ε-$VOPO_4$ may get closer to form a cluster of localized electrons.

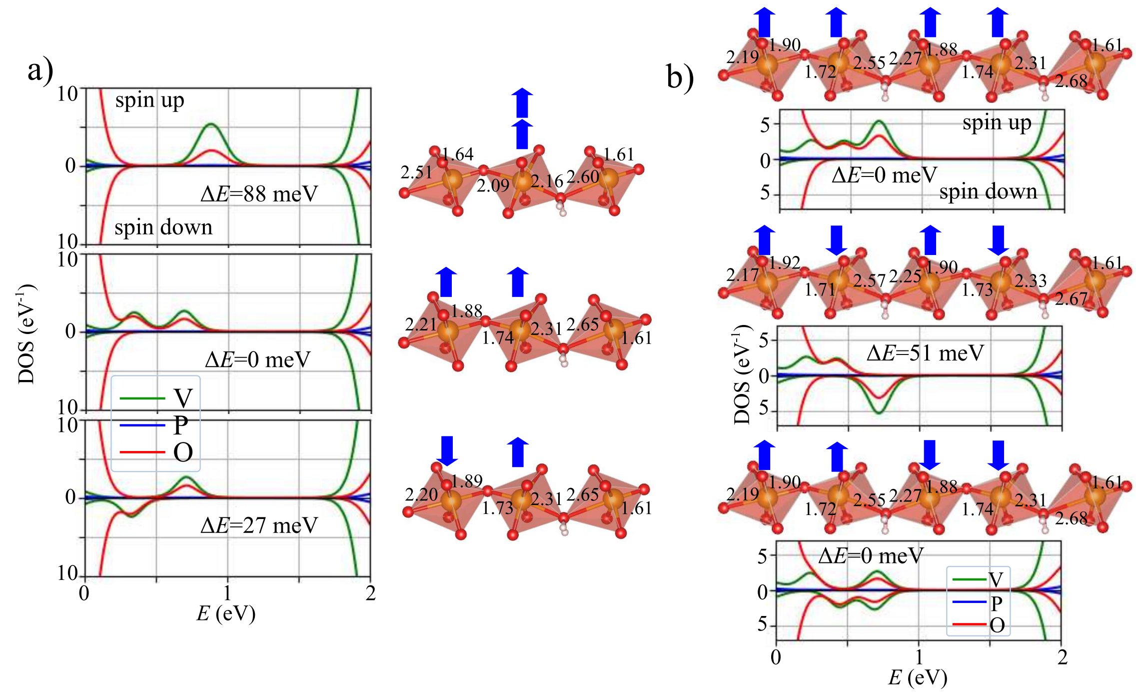

Figure 4: Spin-polarized atom-projected density of states and optimized structure of VO_6 octahedrons in ε-$VOPO_4$ with a) one hydrogen gas and b) two hydrogen gases dopants. Blue arrows denote localized excess electrons. The bond lengths of V-O are presented in units of Å. ΔE is the total energy difference between configurations. The valance band maximum is set to zero in the density of states.

Doping of H_2 molecules

We attempted to start with different setup of initial spin configurations and local bond lengths as described in the section of Computational Methods. In total, we found three configurations of different spin orientations of two localized electrons by doping H_2 molecules to the corner oxygen site as shown in Figure 4 (a). However, we did not find any single configuration with the H_2 molecule lying at the center of two spins. The model in the middle panel has 49 meV lower total energy than the one in the top panel in Figure 3. Consequently, configuration for H_2 molecule doping is more stable by keeping the 2 H interstitial defects on the same oxygen. The top panel show that two electrons are localized on one V-d with almost equal axial V-O bond lengths (2.09 and 2.16 Å). The two electrons have the same spin by Hund's rule. However, the more stable state has a lower total energy of 88 meV, where two electrons are localized on two V-d in adjacent two octahedrons, leading to FM ordering (see the middle panel in Figure 4 (a)). There are two defect states above the valance band maximum. The lower (higher) energy spin up state corresponds to localized electron on octahedron far from (close to) the interstitial H_2. The eigenvalue difference of 0.5 eV between the two states is attributed to anisotropic octahedron distortions. As a comparison, the AFM ordering increases total energy by 27 meV (see the bottom panel in Figure 4 (a)). As shown in Fig. 4 (a), the defect state comprises of notable O-p states. The local magnetic moments on both V-d are close to 1 μ_B indicating half filling by H_2 doping. These indicate that the spin-spin interaction can be described by superexchange mechanism. Based on the Goodenough-Kanamori rules,[31–33] it prefers AFM (FM) ordering when cation-anion-cation bond angle is 180 (90)°. However, V-O-V bond angle is 148° in ε-$VOPO_4$. This may result in a lower energy of FM ordering. Such an exchange energy raised from the spin-spin interaction is comparable to thermal energy at room temperature (26 meV), indicating that a short-range ferromagnetism below the room temperature can be achieved by H_2 doping.

We further investigated the spin-spin interaction upon two H_2 doping. In total, we tested three configurations: (i) two interstitial H_2 near two corner (axial) oxygens at one octahedron, (ii) two interstitial H_2 near corner oxygens at two octahedrons in separated 1D VO_6 octahedron chains, and (iii) two interstitial H_2 near corner oxygens at two separated octahedrons in the same 1D chain. To avoid confusion, (i) and (ii) are not shown, and we only display (iii) in Figure 4 (b). The configurations (i) and (ii) have respectively $\sim$0.5 eV higher and $\sim$0.1 eV lower total energy than configuration (iii). This suggests that H_2 molecules in ε-$VOPO_4$ prefer a dispersion rather than an aggregation, unlike two H doping.

Figure 4 (b) shows the third configuration with three possible spin orientations. In the comparison between FM (the upper panel) and AFM ordering I (the middle panel), FM ordering lowers the total energy by 52 meV. The energy is gained from the spin-spin interaction between localized electrons on two adjacent octahedrons on the left side of interstitial H_2. In the comparison between FM (the upper panel) and AFM ordering II (the bottom panel), the total energies are the same, indicating no spin-spin interaction between two adjacent octahedrons cross the interstitial H_2. Our results suggest that the spin-spin interaction induced by H_2 doping is limited to two adjacent octahedrons. Therefore, we conclude that the doping H_2 to ε-$VOPO_4$ will be homogeneous distributed to the bulk. And the resulting spins only interacts locally.

Doping of single Li atom

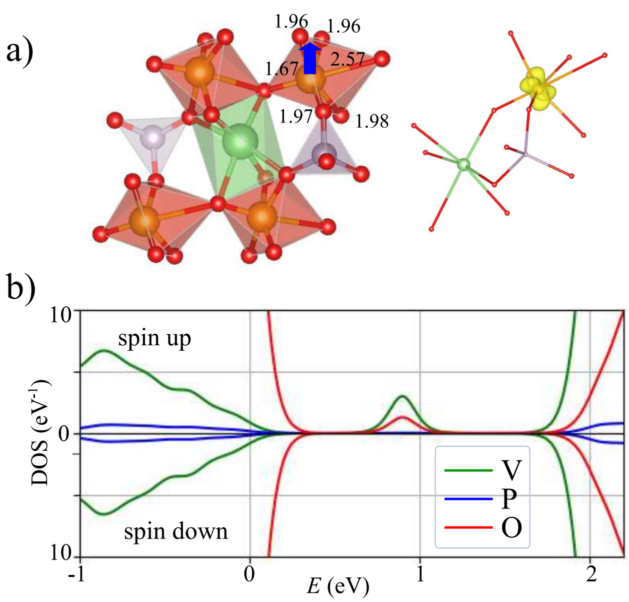

Figure 5: a) Optimized structure of VO_6 octahedrons in ε-$VOPO_4$ with Li dopant. Blue arrow denotes localized excess electron by Li doping. The bond lengths of V-O are presented in units of Å. Spin density associated with the V-d state is presented. b) Spin-polarized atom-projected density of states. The valance band maximum is set to zero. Lithium projected density of states are not shown here due to their absent in the selected energy range.

Figure 5 shows the case of Li doping on the center of 1D cavity. Like H doping, the electrons are localized on V-d in a VO_6 octahedron that is adjacent to the lithium dopant. However, Li doping increases four equatorial V-O bond lengths, whereas H doping distorts the axial V-O bonds. Unlike that the defect state in H doping is mainly contributed from V-d_{yz} orbital at the valance band maximum, the defect state upon Li doping is mainly contributed from V-$d_{x^2-y^2}$ orbital at $\sim$0.6 eV higher than the valance band maximum. Such differences suggest that the extra electrons are trapped efficiently by axial V-O distortion, which may not be preferred by Li doping.

SUMMARY AND CONCLUSIONS

According to thermodynamics, the formation energy of defect X (H, Li) is defined by

$$E^f[X] = E_{\text{tot}}[X] - E_{\text{tot}}[\text{Host}] - n\mu, \tag{1}$$

where $E_{\text{tot}}[X]$ is the total energy of the supercell with defect X, $E_{\text{tot}}[\text{Host}]$ is the total energy of the defect-free supercell, n is the number of defect, and μ is the chemical potential in H- or Li-rich condition. Using this equation, we obtained the formation energies of -1.25, -2.65, and -3.38 eV for H, H_2, and Li interstitial doping, respectively. The results indicate that formation of H or Li interstitial defects in ε-$VOPO_4$ is more favored.

We have shown that doping H, H_2 and Li can localize excess electrons to generate local magnetic moment on V-d orbitals. The local magnetic moments have a spin-spin interaction and they introduce the magnetism to the pristine ε-VPO_5. Our systematic study shows that the spin-spin interaction is limited to two adjacent octahedrons by H_2 doping. Therefore, a long-range magnetic ordering is not plausible by doping of the light elements in ε-VPO_5.

However, it is suggested that the localized spins of dopant ion interact with the charge carriers resulting in a magnetic polarization of the surrounding local moments.[34,35] In that case, the oxygen vacancy can supply spin carriers to interact with local moments as long as the defect level is shallow.[13] While we are still not clear about the defects' formation in ε-VPO_5, we propose three key findings might be applied to advance the carrier-mediated magnetism. First, the localized defect states near the valance band maximum are composed of V-d and O-p. The sizeable O-p characters may facilitate an exchange interaction between V-d and p spin carriers. Second, the short-range spin-spin interactions resulting from the H_2 doping were limited to the 1D chain of VO_6 octahedrons. The 1D character might be applicable for controls magnetic anisotropy.[36] Last, the H dopants prefer to form a cluster, whereas H_2 molecules prefer to be dispersed. Thus, doping H_2 molecules might be suitable for the homogeneous magnetization in ε-VPO_5. Our work provide insight into the magnetic properties of light elements doped ε-VPO_5 and can be useful in the field of spintronics.

Acknowledgments

We acknowledge the NSF (I-DIRSE-IL: 1940272) and NASA (80NSSC19M0152) for their financial supports. The computing resources are provided by XSEDE (TG-DMR180040).

References

(1) Pillai, U. R.; Sahle-Demessie, E. Vanadium phosphorus oxide as an efficient catalyst for hydrocarbon oxidations using hydrogen peroxide. *New J. Chem.* **2003**, *27*, 525–528.

(2) Hutchings, G. J.; Desmartin-Chomel, A.; Olier, R.; Volta, J.-C. Role of the product in the transformation of a catalyst to its active state. *Nature* **1994**, *368*, 41–45.

(3) Savary, L.; Saussey, J.; Costentin, G.; Bettahar, M.; Gubelmann-Bonneau, M.; Lavalley, J. Propane oxydehydrogenation reaction on a VPO/TiO_2 catalyst. Role of the nature of acid sites determined by dynamic in-situ IR studies. *Catal. Today* **1996**, *32*, 57–61.

(4) Ling, C.; Zhang, R.; Mizuno, F. Phase stability and its impact on the electrochemical performance of $VOPO_4$ and $LiVOPO_4$. *J. Mater. Chem. A* **2014**, *2*, 12330–12339.

(5) Lin, Y.-C.; Wen, B.; Wiaderek, K. M.; Sallis, S.; Liu, H.; Lapidus, S. H.; Borkiewicz, O. J.; Quackenbush, N. F.; Chernova, N. A.; Karki, K., et al. Thermodynamics, kinetics and structural evolution of ε-$LiVOPO_4$ over multiple lithium intercalation. *Chem. Mater.* **2016**, *28*, 1794–1805.

(6) Zhou, H.; Shi, Y.; Xin, F.; Omenya, F.; Whittingham, M. S. ε-and β-$LiVOPO_4$: Phase transformation and electrochemistry. *ACS Appl. Mater. Interfaces* **2017**, *9*, 28537–28541.

(7) Whittingham, M. S. Ultimate limits to intercalation reactions for lithium batteries. *Chem. Rev.* **2014**, *114*, 11414–11443.

(8) Shi, Y.; Zhou, H.; Seymour, I. D.; Britto, S.; Rana, J.; Wangoh, L. W.; Huang, Y.; Yin, Q.; Reeves, P. J.; Zuba, M., et al. Electrochemical performance of nanosized disordered $LiVOPO_4$. *ACS omega* **2018**, *3*, 7310–7323.

(9) Esquinazi, P. D.; Hergert, W.; Stiller, M.; Botsch, L.; Ohldag, H.; Spemann, D.; Hoffmann, M.; Adeagbo, W. A.; Chassé, A.; Nayak, S. K., et al. Defect-induced magnetism in nonmagnetic oxides: basic principles, experimental evidence, and possible devices with ZnO and TiO_2. *Phys. Status Solidi B* **2020**, *257*, 1900623.

(10) Akshay, V.; Arun, B.; Mandal, G.; Vasundhara, M. Structural, optical and magnetic behavior of sol-gel derived Ni-doped dilute magnetic semiconductor TiO_2 nanocrystals for advanced functional applications. *Phys. Chem. Chem. Phys.* **2019**, *21*, 2519–2532.

(11) Verma, K. C.; Kotnala, R. Oxygen vacancy induced by La and Fe into ZnO nanoparticles to modify ferromagnetic ordering. *J. Solid State Chem.* **2016**, *237*, 211–218.

(12) Santara, B.; Pal, B.; Giri, P. Signature of strong ferromagnetism and optical properties of Co doped TiO_2 nanoparticles. *J. Appl. Phys.* **2011**, *110*, 114322.

(13) Wang, Q.; Sun, Q.; Jena, P.; Kawazoe, Y. Magnetic properties of transition-metal-doped $Zn_{1-x}T_xO$ (T= Cr, Mn, Fe, Co, and Ni) thin films with and without intrinsic defects: a density functional study. *Phys. Rev. B* **2009**, *79*, 115407.

(14) Iyer, V. B.; Goddard III, W. A. Electrochemical performance and structures of

chromium and molybdenum-doped ε-Li_xVOPO_4 predicted as promising cathodes for next generation lithium-ion batteries. *J. Phys. Chem. C* **2020**, *125*, 275–282.

(15) Benecha, E.; Lombardi, E. Clustering and spin interactions in Fe-doped diamond. *J. Phys. Conf. Ser.* **2017**, *905*, 012033.

(16) Kulish, V. V.; Huang, W. Single-layer metal halides MX_2 (X= Cl, Br, I): stability and tunable magnetism from first principles and Monte Carlo simulations. *J. Mater. Chem. C* **2017**, *5*, 8734–8741.

(17) Yin, X.; Wang, Y.; Jacobs, R.; Shi, Y.; Szlufarska, I.; Morgan, D.; Wang, X. Massive vacancy concentration yields strong room-temperature ferromagnetism in two-dimensional ZnO. *Nano Lett.* **2019**, *19*, 7085–7092.

(18) Adeagbo, W.; Fischer, G.; Ernst, A.; Hergert, W. Magnetic effects of defect pair formation in ZnO. *J. Phys.: Condens. Matter* **2010**, *22*, 436002.

(19) Jain, A.; Ong, S. P.; Hautier, G.; Chen, W.; Richards, W. D.; Dacek, S.; Cholia, S.; Gunter, D.; Skinner, D.; Ceder, G., et al. Commentary: The Materials Project: A materials genome approach to accelerating materials innovation. *APL Mater.* **2013**, *1*, 011002.

(20) Wen, B.; Wang, Q.; Lin, Y.; Chernova, N. A.; Karki, K.; Chung, Y.; Omenya, F.; Sallis, S.; Piper, L. F.; Ong, S. P., et al. Molybdenum substituted vanadyl phosphate ε-$VOPO_4$ with enhanced two-electron transfer reversibility and kinetics for lithium-ion batteries. *Chem. Mater.* **2016**, *28*, 3159–3170.

(21) Blöchl, P. E. Projector augmented-wave method. *Phys. Rev. B* **1994**, *50*, 17953.

(22) Kresse, G.; Furthmüller, J. Efficient iterative schemes for ab initio total-energy calculations using a plane-wave basis set. *Phys. Rev. B* **1996**, *54*, 11169.

(23) Kresse, G.; Joubert, D. From ultrasoft pseudopotentials to the projector augmented-wave method. *Phys. Rev. B* **1999**, *59*, 1758.

(24) Perdew, J. P.; Burke, K.; Ernzerhof, M. Generalized gradient approximation made simple. *Phys. Rev. Lett.* **1996**, *77*, 3865.

(25) Bianchini, M.; Ateba-Mba, J.; Dagault, P.; Bogdan, E.; Carlier, D.; Suard, E.; Masquelier, C.; Croguennec, L. Multiple phases in the ε-VPO_4O-$LiVPO_4O$-Li_2VPO_4O system: a combined solid state electrochemistry and diffraction structural study. *J. Mater. Chem. A* **2014**, *2*, 10182–10192.

(26) Girgsdies, F.; Dong, W.-S.; Bartley, J. K.; Hutchings, G. J.; Schlögl, R.; Ressler, T. The crystal structure of ε-$VOPO_4$. *Solid State Sci.* **2006**, *8*, 807–812.

(27) Kang, B.; Biswas, K. Carrier self-trapping and luminescence in intrinsically activated scintillator: cesium hafnium chloride (Cs_2HfCl_6). *J. Phys. Chem. C* **2016**, *120*, 12187–12195.

(28) Kang, B.; Biswas, K. Exploring polaronic, excitonic structures and luminescence in $Cs_4PbBr_6/CsPbBr_3$. *J. Phys. Chem. Lett.* **2018**, *9*, 830–836.

(29) Xiong, K.; Robertson, J. Hydrogen-induced defects and degradation in oxide ferroelectrics. *Appl. Phys. Lett.* **2004**, *85*, 2577–2579.

(30) Mo, L.-B.; Wang, Y.; Bai, Y.; Xiang, Q.-Y.; Li, Q.; Yao, W.-Q.; Wang, J.-O.; Ibrahim, K.; Wang, H.-H.; Wan, C.-H., et al. Hydrogen impurity defects in rutile TiO_2. *Sci. Rep.* **2015**, *5*, 1–7.

(31) Goodenough, J. B. Theory of the role of covalence in the perovskite-type manganites [La,M(II)] MnO_3. *Phys. Rev.* **1955**, *100*, 564.

(32) Goodenough, J. B. An interpretation of the magnetic properties of the perovskite-type mixed crystals $La_{1-x}Sr_xCoO_{3-\lambda}$. *J. Phys. Chem. Solids* **1958**, *6*, 287–297.

(33) Kanamori, J. Superexchange interaction and symmetry properties of electron orbitals. *J. Phys. Chem. Solids* **1959**, *10*, 87–98.

(34) Dietl, T.; Ohno, o. H.; Matsukura, a. F.; Cibert, J.; Ferrand, e. D. Zener model description of ferromagnetism in zinc-blende magnetic semiconductors. *science* **2000**, *287*, 1019–1022.

(35) Samanta, A.; Goswami, M.; Mahapatra, P. Magnetic and electric properties of Ni-doped ZnO nanoparticles exhibit diluted magnetic semiconductor in nature. *J. Alloys Compd.* **2018**, *730*, 399–407.

(36) Sakamoto, S.; Zhao, G.; Shibata, G.; Deng, Z.; Zhao, K.; Wang, X.; Nonaka, Y.; Ikeda, K.; Chi, Z.; Wan, Y., et al. Anisotropic spin distribution and perpendicular magnetic anisotropy in a layered ferromagnetic semiconductor $(Ba,K)(Zn,Mn)_2As_2$. *ACS Appl. Electron. Mater.* **2021**, *3*, 789–794.

TOC Graphic